Reduced-Complexity Detectors for Multi-*h* CPM in Aeronautical Telemetry

ERIK PERRINS, Senior Member, IEEE
University of Kansas

MICHAEL RICE, Senior Member, IEEE
Brigham Young University

A two-index, partial response continuous-phase modulation (CPM) known as ARTM CPM was adopted for use in aeronautical telemetry in the IRIG 106 standard in 2004. This waveform was selected because it achieves approximately three times the spectral efficiency of PCM/FM, the legacy modulation in IRIG-106. However, the optimum receiver requires 128 real-valued matched filters and keeps track of the waveform state with a trellis of 512 states and 2048 branches. Various complexity-reducing techniques are applied and the resulting loss in detection efficiency is quantified. It is shown that the full 512-state trellis is not required to achieve desirable detection efficiency: two different 32-state configurations were found to perform within 0.05 dB of optimal; two different 16-state configurations were found to perform within 0.80 dB of optimal; and an 8-state configuration was found to perform within 1.05 dB of optimal. The analysis and simulation results show that to achieve a given state complexity, proper combination of two or more complexity-reducing techniques generally outperforms the use of a single complexity-reducing technique.

Manuscript received August 5, 2005; revised March 8, 2006; released for publication June 24, 2006.

IEEE Log No. T-AES/43/1/895035.

Refereeing of this contribution was handled by T. F. Roome.

This paper was presented in part at the International Telemetering Conference (ITC), San Diego, CA, Oct. 2004.

Authors' addresses: E. Perrins, Dept. of Electrical Engineering and Computer Science, University of Kansas, Lawrence, KS 66045, E-mail: (esp@ieee.org); M. Rice, Dept. of Electrical and Computer Engineering, Brigham Young University, Provo, UT 84602, E-mail: (mdr@ee.byu.edu).

I. INTRODUCTION

PCM/FM has been the dominant carrier for aeronautical telemetry since the 1970s. Spectrum reallocations of frequency bands in 1997 prompted a migration away from PCM/FM to more bandwidth-efficient waveforms [1]. Size, weight, and power supply constraints force the use of fully saturated, nonlinear RF power amplifiers. As a consequence, the search for more bandwidth-efficient waveforms has been limited to constant envelope waveforms. By 2004, a pair of interoperable waveforms, Feher-patented QPSK (FQPSK) [2] and a version of shaped offset QPSK designated SOQPSK-TG [3], were adopted in the IRIG 106 standard [4]. These waveforms achieve twice the spectral efficiency of PCM/FM even with nonlinear amplifiers [5] while maintaining the same detection efficiency of PCM/FM with limiter-discriminator detection.

Recently, a partial response, multi-*h* CPM, denoted ARTM CPM, was adopted as part of the IRIG-106 standard [6]. This waveform achieves almost three times the spectral efficiency of PCM/FM while promising the same detection efficiency as PCM/FM with limiter-discriminator detection. The spectral improvement is realized at the expense of complexity. The optimum detector requires 128 real-valued matched filters together with a trellis consisting of 512 states and 2048 branches. Thus, complexity-reducing approximations that result in only minor decreases in detection efficiency are of tremendous importance.

This paper analyzes the performance of some well-known complexity-reducing techniques and quantifies the corresponding performance degradations. The surveyed techniques include:

1) frequency pulse truncation [7, 8],
2) state-space partitioning (SSP) [9],
3) pulse amplitude modulation (PAM) [10, 11],
4) orthogonal basis functions [12].

While these complexity-reducing techniques show promise when applied individually, it is shown that for ARTM CPM the best results are obtained with detectors based on a combination of these techniques. For example, using a combined complexity-reduction approach it is shown that two different 32-state detectors perform within 0.05 dB of optimum, two different 16-state detectors perform within 0.8 dB of optimum, and one 8-state detector performs slightly more than 1 dB from optimum. On the other hand, when the above approaches are applied individually, the best performing 16-state detector is suboptimum by 1.6 dB. It is not clear from previously published work that results such as these were ever anticipated.

The paper is organized as follows. The parameters of ARTM CPM and the maximum likelihood detector are described in Section II. Complexity-reduction

TABLE I
Parameters Defining ARTM CPM

Symbol Values	$\alpha_i \in \{-3,-1,+1,+3\}$
Partial Response	$L = 3$
Frequency Pulse	$f(t) = \begin{cases} \frac{1}{2LT}\left[1-\cos\left(\frac{2\pi t}{LT}\right)\right] & 0 \le t \le LT \\ 0 & \text{otherwise} \end{cases}$
Modulation Indexes	$h_i \in \{\frac{4}{16}, \frac{5}{16}\}$

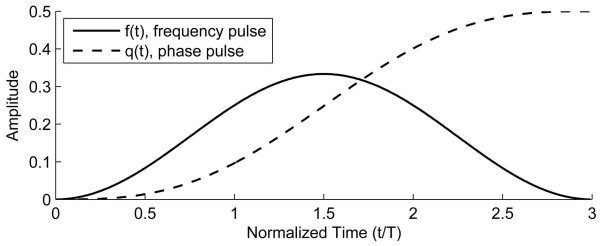

Fig. 1. Length-3T raised cosine (3RC) frequency pulse and corresponding phase pulse for ARTM CPM.

techniques are summarized and applied in Section III. The various separate techniques are combined in Section IV where good and bad combinations are explored. The paper ends with a summary and conclusion.

II. ARTM CPM

A. Signal Model

The complex baseband CPM signal may be represented as [13]

$$s(t;\boldsymbol{\alpha}) = \exp\{j\phi(t;\boldsymbol{\alpha})\} \tag{1}$$

where the phase is a pulse train of the form

$$\phi(t;\boldsymbol{\alpha}) = 2\pi \sum_i h_i \alpha_i q(t - iT) \tag{2}$$

where α_i is an M-ary symbol, T is the symbol time, h_i is the digital modulation index used during the ith interval that cycles through a set of N_h possibilities, and $q(t)$ is the phase pulse which is usually thought of as the time-integral of a frequency pulse $f(t)$ with area 1/2. The specific values that define ARTM CPM are listed in Table I. The frequency pulse $f(t)$ and the corresponding phase pulse $q(t)$ are plotted in Fig. 1.

During the interval corresponding to the nth symbol, $nT \le t \le (n+1)T$, the phase may be expressed as

$$\phi(t;\boldsymbol{\alpha}) = \underbrace{2\pi \sum_{i=n-2}^{n} h_i \alpha_i q(t - iT)}_{\theta(t;\boldsymbol{\alpha}_n)} + \underbrace{\pi \sum_{i=0}^{n-3} h_i \alpha_i}_{\vartheta_{n-3}} \tag{3}$$

where

$$\boldsymbol{\alpha}_n = \alpha_{n-2}, \alpha_{n-1}, \alpha_n \tag{4}$$

is the correlative state vector which contains the $L = 3$ most recent symbols. These three symbols determine the phase trajectory taken by $\theta(t;\boldsymbol{\alpha}_n)$ in (3) during the interval $nT \le t \le (n+1)T$. There are $M^L = 4^3 = 64$ possible values the correlative state vector can assume, each resulting in a different phase trajectory.

The second term in (3), ϑ_{n-3}, is called the cumulative phase and represents the contribution to the carrier phase from all symbols that have worked their way through the frequency pulse and now contribute a constant value to the overall phase. Since there are two modulation indexes with values 4/16 and 5/16, it can be shown that ϑ_{n-3} has 32 possible values $0, \pi/16, 2\pi/16, \ldots, 31\pi/16$.

B. Maximum Likelihood Detection

Let

$$r(t) = \exp\{\phi(t;\boldsymbol{\alpha})\} + w(t) \tag{5}$$

be the received signal where $w(t)$ is a complex-valued Gaussian random process whose real and imaginary parts are uncorrelated zero-mean random processes each with power spectral density $N_0/2$ W/Hz. The maximum likelihood detector outputs the symbol sequence

$$\hat{\boldsymbol{\alpha}} = \arg\min_{\boldsymbol{\alpha}} \left\{ \int |r(t) - e^{j\phi(t;\boldsymbol{\alpha})}|^2 dt \right\}. \tag{6}$$

Expanding the right-hand side of this rule and ignoring terms that do not depend on the data produces an alternate, more workable form, for the decision rule:

$$\hat{\boldsymbol{\alpha}} = \arg\max_{\boldsymbol{\alpha}} \left\{ \mathrm{Re}\left[\int r(t) e^{-j\phi(t;\boldsymbol{\alpha})} dt \right] \right\}. \tag{7}$$

The right-hand side of (7) may be expressed recursively for use with the Viterbi algorithm [13, ch. 7]. At time $t = nT$ we have

$$\begin{aligned} &\underbrace{\mathrm{Re}\left[\int_0^{(n+1)T} r(t) e^{-j\phi(t;\boldsymbol{\alpha})} dt \right]}_{\lambda(n)} \\ &\quad = \underbrace{\mathrm{Re}\left[\int_0^{nT} r(t) e^{-j\phi(t;\boldsymbol{\alpha})} dt \right]}_{\lambda(n-1)} + \mathrm{Re}\left[\int_{nT}^{(n+1)T} r(t) e^{-j\phi(t;\boldsymbol{\alpha})} dt \right]. \end{aligned} \tag{8}$$

Using (3), the last term in (8) may be expressed as

$$\begin{aligned} &\mathrm{Re}\left[\int_{nT}^{(n+1)T} r(t) e^{-j\phi(t;\boldsymbol{\alpha})} dt \right] \\ &\quad = \mathrm{Re}\left[e^{-j\vartheta_{n-3}} \int_{nT}^{(n+1)T} r(t) e^{-j\theta(t;\boldsymbol{\alpha}_n)} dt \right]. \end{aligned} \tag{9}$$

The relationships (8) and (9) suggest the receiver structure shown in Fig. 2. During the interval $nT \le t \le (n+1)T$, the received signal is correlated with

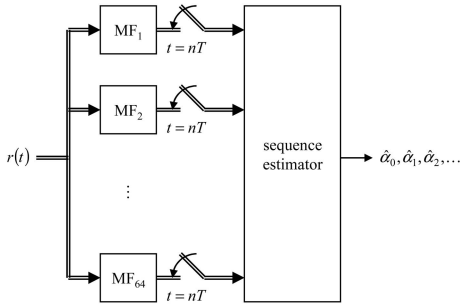

Fig. 2. CPM detector showing matched filters and the use of sampled matched filter outputs for sequence detection.

the $M^L = 64$ possible values of $\exp\{j\theta(t;\boldsymbol{\alpha}_n)\}$ by the 64 matched filters (MFs) as shown. The matched filter outputs are rotated by the possible values of the cumulative phase ϑ_{n-3} and used to update the partial path metrics in a trellis with $32 \times M^{L-1} = 512$ states and $32 \times M^L = 2048$ branches. Note that each state has a unique state vector of the form

$$\sigma = \{\vartheta_{n-3}, \alpha_{n-2}, \alpha_{n-1}\}. \tag{10}$$

In the next section, it is shown that only half of the 32 values of the cumulative phase need to be represented in the state vector.

The computational requirements for the detector are summarized by the number of matched filters (or correlators) and the number of trellis states. The 64 complex-valued matched filters correspond to 256 real-valued matched filters. Half of these filters may be eliminated (through dual use) using the symmetry properties of cosine and sine. In the end, the maximum likelihood detector requires 128 real-valued matched filters together with a trellis consisting of 512 states.

The probability of bit error may be quantified using the union bound with pairwise error probabilities. It was shown in [13, ch. 2], that the probability of bit error for maximum likelihood sequence detection (MLSD) is

$$P_b \le \sum_{l=0}^{\infty} C_l Q\left(\sqrt{d_l^2 \frac{E_b}{N_0}}\right) \tag{11}$$

where

$$Q(x) = \frac{1}{\sqrt{2\pi}} \int_x^{\infty} e^{-u^2/2} du \tag{12}$$

E_b is the equivalent bit energy, and the constants d_l and C_l are associated with different mergers, or error events, in the trellis. Evaluation of (11) requires knowledge of the set of distances between all possible waveforms. The distance between the waveforms corresponding to the sequences $\boldsymbol{\alpha}_1$ and $\boldsymbol{\alpha}_2$ is

$$d^2 = \frac{1}{2E_b} \int_{(R+L-1)T} |s(t;\boldsymbol{\alpha}_1) - s(t;\boldsymbol{\alpha}_2)|^2 dt \tag{13}$$

where the difference between $\boldsymbol{\alpha}_1$ and $\boldsymbol{\alpha}_2$ is non-zero for a span of R symbols and the interval of integration is related to this interval. For ARTM CPM, the sequences which satisfy

$$\boldsymbol{\alpha}_1 - \boldsymbol{\alpha}_2 = \ldots, 0, 2, -4, 6, -4, 2, 0, \ldots \tag{14}$$

and

$$\boldsymbol{\alpha}_1 - \boldsymbol{\alpha}_2 = \ldots, 0, 2, -2, 0, 2, -2, 0, \ldots \tag{15}$$

have the two smallest distances.[1] The coefficient C_l is given by

$$C_l = \frac{W_l N_l}{\log_2(M) N_h M^R} \tag{16}$$

where W_l is the the number of bit errors associated with the trellis path pairs that differ by d_l, N_l is the number of trellis path pairs that differ by d_l, and $N_h = 2$ is the number of modulation indexes. There are 72 sequence pairs that satisfy (14); they have a squared distance $d^2 = 1.288$ and correspond to 7 bit errors. There are 648 sequence pairs that satisfy (15); they have a squared distance of $d^2 = 1.656$ and correspond to 4 bit errors. Using the first two terms in (11) produces the approximation

$$P_b \approx \frac{(7)(72)}{(2)(2)(4^5)} Q\left(\sqrt{1.288 \frac{E_b}{N_0}}\right) + \frac{(4)(648)}{(2)(2)(4^5)} Q\left(\sqrt{1.656 \frac{E_b}{N_0}}\right). \tag{17}$$

The computational burden in the detector can be reduced by proper selection of approximations that reduce the number of matched filters, trellis states, or both. Each of these complexity-reducing techniques is accompanied by an increase in the signal-to-noise ratio (SNR) required to achieve a target bit error rate. The complexity/SNR trade-off is the subject of the remainder of this paper.

III. COMPLEXITY-REDUCING TECHNIQUES

A. Tilted Phase

The first complexity-reducing technique that can be applied is the "tilted phase" technique described by Rimoldi [14]. For this method, we use the data symbols $U_i = (\alpha_i + M - 1)/2$ in place of the original data α_i when defining the cumulative phase; therefore, we have

$$\vartheta_{n-3} = \pi \sum_{i=0}^{n-3} h_i \alpha_i = \nu_{n-3} + \underbrace{2\pi \sum_{i=0}^{n-3} h_i U_i}_{\theta_{n-3}} \tag{18}$$

[1] These two difference sequences are non-zero over a span of $R = 5$ symbols. They produce CPM signals that are different over an interval limited to $R + L = 7$ symbol times. There are sequence pairs for which $R < 5$, but the resulting signals have larger distances. There are also sequence pairs with $R > 5$ where the distance accumulates very slowly. In these cases, the distance in (13) might be small after only 7 symbol times of integration, but it ultimately does surpass the minimum distance upon further integration.

where the data-independent phase tilt is defined as $\nu_i \triangleq \nu_{i-1} - \pi h_i(M-1)$. Note that the substitution $\alpha_i = 2U_i - (M-1)$ is only used for the data symbols in the cumulative phase (and not in the correlative state vector). The data-dependent term in (18) is the phase state, which assumes only half as many values as the cumulative phase. For ARTM CPM, the 16 possible values of the phase state are

$$\theta_{n-3} \in \left\{0, \frac{2\pi}{16}, 2\frac{2\pi}{16}, \ldots, 15\frac{2\pi}{16}\right\}. \tag{19}$$

There is no loss in detection efficiency with this technique. By using only 16 phase states, the number of trellis states is reduced from 512 to 256. The state vector in this case is

$$\sigma = \{\theta_{n-3}, \alpha_{n-2}, \alpha_{n-1}\}. \tag{20}$$

The number of matched filters required remains the same. The tilted phase is assumed for the remainder of the paper.

B. Frequency Pulse Truncation

Another complexity-reducing technique is to form a trellis based on a truncated frequency pulse of length $L'T$, where $L' \leq 3$. This technique was first proposed by Aulin, Sundberg, and Svensson [7] and a nice description can be found in [8] or [13]. This approach is motivated by the observation that the amplitude of the frequency pulse in Fig. 1 is very small at the ends. As an example, by approximating the frequency pulse with a length-$2T$ pulse, the phase trajectory $\theta(t; \alpha_{n-2}, \alpha_{n-1}, \alpha_n)$ is now a function of only α_{n-1} and α_n and can be replaced by a new phase trajectory $\tilde{\theta}(t; \alpha_{n-1}, \alpha_n)$. The contribution of the symbol α_{n-2} is absorbed into the phase state θ_{n-2}. The state vector becomes

$$\sigma = \{\theta_{n-2}, \alpha_{n-1}\}. \tag{21}$$

As a consequence, the number of matched filters is reduced from 128 to 32 and the number of trellis states is reduced from 256 to 64. We point out that this reduction in states is a correlative state reduction, because one coordinate from the correlative state vector has been removed. The metric update equation becomes

$$\lambda(n) = \lambda(n-1) + \mathrm{Re}\left[e^{-j\vartheta_{n-2}} \int_{(n+1/2)T}^{(n+3/2)T} r(t) e^{-j\tilde{\theta}(t;\alpha_{n-1},\alpha_n)} dt\right]. \tag{22}$$

The performance analysis must account for the fact that the signal model used by the demodulator $\tilde{s}(t;\boldsymbol{\alpha})$ is different than the transmitted signal $s(t;\boldsymbol{\alpha})$. The analysis of mismatched detectors was introduced in [7] (see also [8]). It is based on a modified distance measure, the projected Euclidean distance (PED), between the signals corresponding to $\boldsymbol{\alpha}_1$ and $\boldsymbol{\alpha}_2$:

$$\tilde{d} = \frac{1}{\sqrt{2E_b}} \frac{\int |\tilde{s}(t;\boldsymbol{\alpha}_2) - s(t;\boldsymbol{\alpha}_1)|^2 dt - \int |\tilde{s}(t;\boldsymbol{\alpha}_1) - s(t;\boldsymbol{\alpha}_1)|^2 dt}{\sqrt{\int |\tilde{s}(t;\boldsymbol{\alpha}_1) - \tilde{s}(t;\boldsymbol{\alpha}_2)|^2 dt}} \tag{23}$$

where the interval of integration is $(R + L' - 1)T$ and corresponds to the interval where $\boldsymbol{\alpha}_1$ and $\boldsymbol{\alpha}_2$ are different. The probability of error can be bounded using a union bound, similar to (11), where the PED in (23) is used in place of the Euclidean distance d_l in the pairwise error probability. As was the case with the optimal detector, the union bound can be truncated with a finite number of terms. In fact, a good approximation is obtained when the union bound contains only the 72 sequence pairs (transmitted and erroneously detected) that satisfy (14), and also the 648 sequence pairs that satisfy (15), namely

$$P_b \approx \frac{7}{(2)(2)(4^5)} \sum_{k=0}^{71} Q\left(\tilde{d}_k \sqrt{\frac{E_b}{N_0}}\right) + \frac{4}{(2)(2)(4^5)} \sum_{m=0}^{647} Q\left(\tilde{d}_m \sqrt{\frac{E_b}{N_0}}\right). \tag{24}$$

The values of the PED are illustrated in Fig. 3(a) and (b) for $L' = 2$ and $L' = 1$, respectively. In the figure, these distance quantities are given in their squared form for easy comparison with the optimal squared distances (dashed lines in the figures). In general, however, there is no guarantee that the PED is a positive quantity (an example where the PED is negative is given in Section IIID). For this reason it is used in (24) as an unsquared quantity. These plots illustrate the effect of frequency pulse truncation on performance. For $L' = 2$, there are some paths with a squared PED as low as 1.22 (note there are other paths with a squared PED of 1.37). For $L' = 1$, there are some paths with a squared PED as small as 0.32.

The bit error rate performance for this approximation is shown in Fig. 4. Observe that the simulation results coincide with the approximation (24) for large E_b/N_0 but are different for small E_b/N_0. (This is to be expected since truncated union bounds are only accurate asymptotically.) The $L' = 2$ approximation results in a very small loss, while the $L' = 1$ results in a much larger loss. The performance/complexity trade-off is summarized in Table II. The $L' = 2$ approximation was used in the results reported for ARTM CPM in [15].

C. State-Space Partitioning

SSP was applied to detection of partial response CPM by Larsson [9]. This is a special case of an approach referred to as SA(B,C) with $B = 1$ [16, 17]. In many instances, the detectors that result from SSP

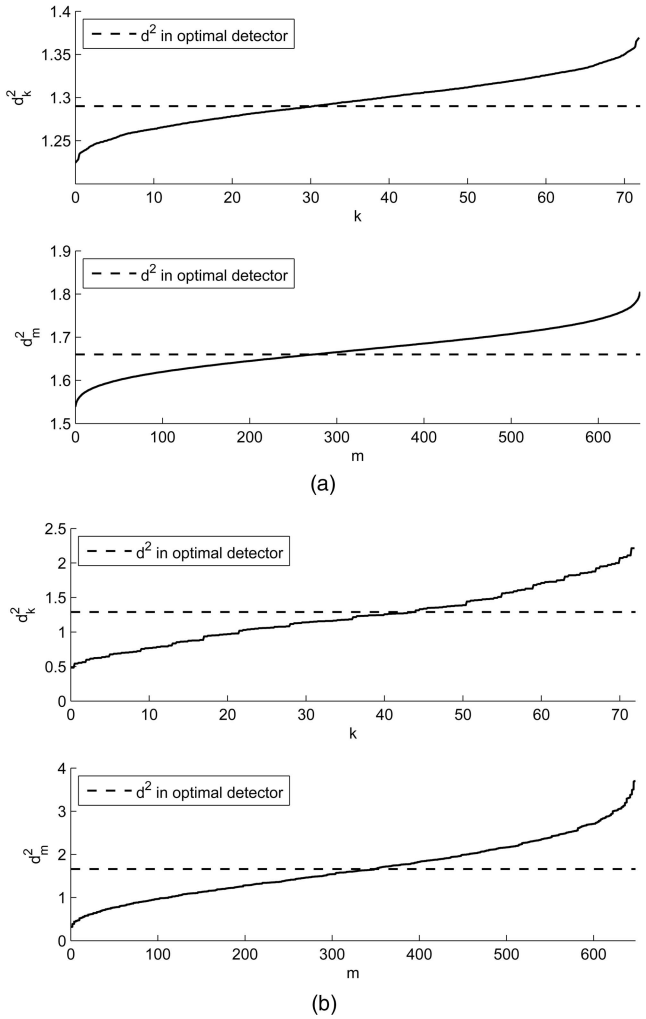

Fig. 3. Values of squared PED for frequency pulse truncation with (a) $L' = 2$ and (b) $L' = 1$. These values are used in (24).

TABLE II
Performance/Complexity Trade-Off for Frequency Pulse Truncation Approximation

L'	Number of States	Number of MFs	Loss (dB) at $P_b = 10^{-5}$
3	256	128	—
2	64	32	0.02
1	16	8	4.10

can be implemented with reduced state sequence detection (RSSD) [9], which is a decision feedback scheme that was developed in [18]. We first summarize the concept behind the SSP approach and then apply the approach to ARTM CPM.

The basic idea is to map each possible CPM state vector in (20) onto a corresponding label vector

$$\epsilon = \mathbf{\Gamma}(\sigma) = \{\epsilon_{n-3}, \epsilon_{n-2}, \epsilon_{n-1}\} \tag{25}$$

$$= \{\Gamma^{(\gamma_3)}(\theta_{n-3}), \Gamma^{(\gamma_2)}(\alpha_{n-2}), \Gamma^{(\gamma_1)}(\alpha_{n-1})\} \tag{26}$$

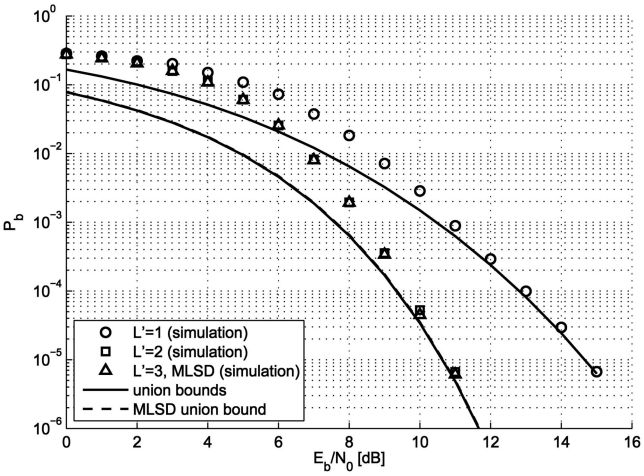

Fig. 4. Performance of detectors with frequency pulse truncation with $L' = 1$, $L' = 2$, and $L' = 3$ (MLSD).

where the scalar function $\Gamma^{(\gamma_k)}(\cdot)$ operates on a single data symbol or phase state and takes on values in the range $0, 1, \ldots, \gamma_k - 1$. For example, the partition

$$\Gamma^{(2)}(\theta) \triangleq [0\ 1\ 0\ 1\ 0\ 1\ 0\ 1\ 0\ 1\ 0\ 1\ 0\ 1\ 0\ 1] \tag{27}$$

maps the 16 original phase states to one of two possible values. Therefore, we are simply relabeling (partitioning) the states in the trellis. When we map multiple CPM states onto the same label vector, we reduce the number of states in the detector to

$$N_S(\mathbf{\Gamma}) = \prod_{k=1}^{3} \gamma_k. \tag{28}$$

The problem studied by Larsson is that of optimizing the detector under a joint complexity/error performance criterion [9]. The solutions obtained in [9] and [19] are both systematic and elegant.

The first step in the solution to this problem is to identify the set of critical difference states [9]. A difference state is simply the difference between two CPM states: $\Delta\sigma = \sigma_i - \sigma_j$. A critical difference state is a non-zero difference state that can be reached with a distance that is smaller than the minimum distance. A straightforward algorithm for identifying the critical states is shown in [19, p. 40]. For ARTM CPM, there are 125 difference states that can be reached with a squared distance of less than 1.288; these are the critical difference states. In the case of the optimal detector, these states do not pose a problem since the full trellis is able to resolve the fact that $\Delta\sigma \neq 0$ in each of these cases; therefore, the two competing paths occupy different states in the trellis and do not merge together until some future time when $\Delta\sigma = 0$, which, by definition, cannot occur with a squared distance smaller than the minimum squared distance of 1.288.

The next step in Larsson's solution is to identify the set of "interesting" state-space partitions. These

are found by obtaining the minimal partitions for the respective phase state and data alphabets (minimal partitions are defined in [19] and an algorithm for obtaining them is shown in [19, p. 94]). For ARTM CPM, the 4-ary symbol alphabet has 5 minimal partitions [9] and the 16-ary phase state alphabet has 45 minimal partitions, as determined in this present study. Therefore, there are $45 \times 5 \times 5 = 1125$ distinct state-space partitions for ARTM CPM that are based on these minimal partitions.

The last step in Larsson's solution is to perform the optimization under specific criteria. Two different criteria were proposed in [9]. The first is

$$\text{minimize } N_S(\mathbf{\Gamma}) \text{ subject to } d^2_{\min}(\mathbf{\Gamma}) = 1.288. \quad (29)$$

In other words, minimize the number of trellis states without introducing a new (smaller) minimum distance. Those state-space partitions that violate (29) by lowering the minimum distance, do so by producing $\mathbf{\Gamma}(\Delta\sigma) = 0$ for at least one of the critical difference states. The second trellis optimization criterion proposed in [9] is

$$\text{maximize } d^2_{\min}(\mathbf{\Gamma}) \text{ subject to } N_S(\mathbf{\Gamma}) = N_D. \quad (30)$$

In other words, find the trellis of a desired number of states N_D with the best minimum distance. We now identify the solution to both of these optimization criteria for the case of ARTM CPM.

The smallest trellis with a minimum squared distance of 1.288 [i.e., the solution to (29)] has a 32-state trellis defined by the label vector

$$\epsilon = \{\Gamma^{(2)}(\theta_{n-3}), \Gamma^{(4)}(\alpha_{n-2}), \Gamma^{(4)}(\alpha_{n-1})\} \quad (31)$$

where $\Gamma^{(4)}(\alpha)$ is a trivial partition

$$\Gamma^{(4)}(\alpha) \stackrel{\Delta}{=} [0\ 1\ 2\ 3]. \quad (32)$$

Here the 16 original phase states θ_{n-3} are mapped to one of two possible values by $\Gamma^{(2)}(\theta_{n-3})$, and the 4-ary data symbols α_{n-2} and α_{n-1} are not changed (apart from a mapping to another 4-ary alphabet by $\Gamma^{(4)}(\alpha)$). The actual phase information that is lost via the mapping $\Gamma^{(2)}(\theta_{n-3})$ is reconstructed inside the detector by using decisions from the path history (i.e., decision feedback). Therefore, this detector can be implemented with RSSD. While the minimum squared distance of this detector is 1.288 (which makes the detector asymptotically optimum with large E_b/N_0), the SSP creates several near-minimum-distance/near-critical mergers that produce a noticeable degradation for E_b/N_0 of practical interest.[2] Accordingly, it is not sufficient

[2]This highlights the somewhat unsettling fact, which is confirmed by the numerical results discussed herein, that approaching the complexity-reduction problem using only minimum-distance arguments does not necessarily guarantee the best results.

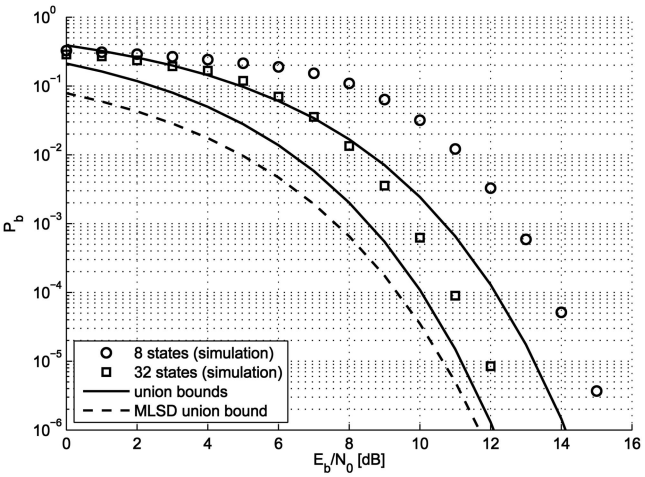

Fig. 5. Performance of detectors with SSP.

to approximate the union bound in (11) with only two terms, as was the case in (17); instead, the error probability is approximated as

$$\begin{aligned} P_b \approx & \frac{(7)(72)}{(2)(2)(4^5)} Q\left(\sqrt{1.288\frac{E_b}{N_0}}\right) \\ & + \frac{(4)(648)}{(2)(2)(4^5)} Q\left(\sqrt{1.656\frac{E_b}{N_0}}\right) \\ & + \frac{(4)(36)}{(2)(2)(4^3)} Q\left(\sqrt{1.43\frac{E_b}{N_0}}\right) \\ & + \frac{(4)(162)}{(2)(2)(4^4)} Q\left(\sqrt{1.53\frac{E_b}{N_0}}\right) \end{aligned} \quad (33)$$

where two more near-minimum-distance terms are added that have relatively large coefficients C_l. The bit error rate performance for this approximation is shown in Fig. 5. Note that the performance approximation in (33) predicts a degradation of 0.5 dB at $P_b = 10^{-5}$; however, the simulation results indicate a loss of 1.3 dB at the same operating point. This is attributable to error propagation due to the decision feedback, since it was observed during the execution of the simulations that the bit error weight of the error events was, at times, an order of magnitude larger than the nominal value of W_l. In Section IV, three different 32-state detectors are identified that significantly outperform this present detector and are all within 0.1 dB of optimum.

The solution to the second optimization criterion in (30) is, of course, dependent on the desired size of the trellis N_D. For ARTM CPM, the analysis shows that the best 16-state trellis has $d^2_{\min}(\mathbf{\Gamma}) = 0.902$, which also turns out to be the best minimum squared distance for a 12-state trellis. A more attractive option to these is the best 8-state trellis, which has $d^2_{\min}(\mathbf{\Gamma}) = 0.895$. The phase states in this trellis are all mapped to one value by the all-zeros partition $\Gamma^{(1)}(\theta_{n-3})$. The

TABLE III
Performance/Complexity Trade-Off for SSP

Design Rule	Number of States	Number of MFs	Loss (dB) at $P_b = 10^{-5}$
Eq. (29)	32	128	1.30
Eq. (30)	8	128	4.00

symbol α_{n-2} is partitioned with

$$\Gamma^{(2)}(\alpha) \triangleq [0\ 1\ 0\ 1] \tag{34}$$

and α_{n-1} is relabeled with the trivial mapping $\Gamma^{(4)}(\alpha)$. Therefore, the 8 states in this detector are defined by

$$\epsilon = \{\Gamma^{(1)}(\theta_{n-3}), \Gamma^{(2)}(\alpha_{n-2}), \Gamma^{(4)}(\alpha_{n-1})\}. \tag{35}$$

Note that this detector can also be implemented with RSSD and its performance is shown in Fig. 5. Although $d^2_{\min}(\mathbf{\Gamma}) = 0.895$, there are five other critical difference states that have $\mathbf{\Gamma}(\Delta\sigma) = 0$ for this detector. Therefore, the union bound in (11) is best approximated by the six terms that represent these mergers:

$$P_b \approx \sum_{l=0}^{5} C_l Q\left(\sqrt{d_l^2 \frac{E_b}{N_0}}\right) \tag{36}$$

where, in order of increasing l, we have $\{d_l^2\} = \{0.895, 0.902, 0.971, 0.976, 1.091, 1.094\}$ and $\{C_l\} = \{9/16, 9/16, 9/16, 9/64, 3/32, 15/32\}$. The value of $d^2_{\min}(\mathbf{\Gamma}) = 0.895$ alone suggests an asymptotic loss of 1.58 dB; however, the approximate union bound above gives a loss of 2.60 dB at $P_b = 10^{-5}$, and the simulation results in Fig. 5 show a loss of 4.0 dB at the same operating point. The discrepancy between the union bound and the simulations results is again ascribed to error propagation from the decision feedback. Also, as with the previously studied 32-state detector, the minimum distance term in the union bound does not become dominant in the E_b/N_0 range of practical interest. Although this 8-state detector optimizes the design criterion in (30), a better performing 8-state detector (approximately 1 dB suboptimum) is found in Section IV. The performance/complexity trade-off for both SSP detectors is summarized in Table III.

D. Pulse Amplitude Modulation Technique

An entirely different viewpoint for CPM is given by the PAM representation, which was first derived for binary single-h CPM by Laruent [20] and later extended to M-ary single-h CPM by Mengali and Morelli [21] and to M-ary multi-h CPM by Perrins and Rice [10]. Using the PAM representation, the ARTM CPM waveform may be expressed as

$$s(t;\boldsymbol{\alpha}) = \sum_{k=0}^{47} \sum_{i} a_{k,i} g_{k,i}(t - iT) \tag{37}$$

where $\{a_{k,i}\}$ is a set of 48 pseudosymbols which modulate the amplitude of the 48 signal pulses $g_{k,i}(t)$.[3] The details required to construct the pseudosymbols and signal pulses are too numerous to give here; a full description is available in [10]. The essential characteristics of these quantities are the following.

1) The signal pulses vary in amplitude and duration.
2) There is one pulse of length $4T$, 2 pulses of length $3T$, 9 pulses of length $2T$, and 36 pulses of length T.
3) The longest pulses (of durations $3T$ and $4T$) have the largest amplitude while the shortest pulses (of duration T) have extremely small amplitude.
4) The set of 48 pseudosymbols can be represented by a 256-state trellis (using the tilted phase) with the state vector (20).
5) Within the set of 48 pseudosymbols, the ones associated with the largest pulses do not require a full 256-state trellis.

The most straightforward approach to complexity reduction is simply to truncate the outer sum in (37). This type of detector was described by Kaleh [22] for binary CPM and Colavolpe and Raheli [23] for nonbinary CPM. The approximate signal resulting from using the first K terms is given by

$$s'(t;\boldsymbol{\alpha}) = \sum_{k=0}^{K-1} \sum_{i} a_{k,i} g_{k,i}(t - iT). \tag{38}$$

The branch metric for this detector is given by

$$\lambda(n) = \lambda(n-1) + \mathrm{Re}\left[\sum_{k=0}^{K-1} z_{k,n} a_{k,n}^*\right] - S_{\boldsymbol{\alpha}_n} \tag{39}$$

where the sampled matched filter output is

$$z_{k,n} = \int_{nT}^{(n+D_k)T} r(t) g_{k,n}(t - nT) dt \tag{40}$$

and $S_{\boldsymbol{\alpha}_n}$ is a bias constant that arises from the fact that the truncation produces approximations that no longer have the same energy (this is explained in greater detail in [11]). The pulses $g_{k,n}(t)$ have a duration of D_k symbol times and the shortest pulse has a duration of $D_{\min} = \min_{0<k<K-1} D_k$.

As K decreases, the approximation error increases, the number of matched filters decreases, and the performance worsens. The state complexity is actually determined by the length of the shortest pulse used in the approximation, $D_{\min}$, and not by the number of pulses used (this nonobvious fact is demonstrated

[3] There are actually 48 pulses for each modulation index. Since there are two modulation indexes, there are $2 \times 48 = 96$ pulses. But, since the modulation indexes alternate between the two possible values (4/16 and 5/16), only one set of 48 pulses or the other is active during a given length-T interval. For this reason, the equivalent PAM representation (37) sums 48 pulses.

in [24]). For this reason, if the truncation includes one pulse of a given length, it should include all pulses of a given length. Therefore, the natural choices for K are 1, 3, 12, and 48.

The mismatched detector analysis described previously is used to analyze the performance of these approximations. For the PAM case, the PED reduces to [11]

$$d' = \frac{1}{\sqrt{2E_b}} \frac{\begin{array}{r} 2\,\mathrm{Re}\int s(t;\boldsymbol{\alpha}_1)[s''(t;\boldsymbol{\alpha}_1) - s''(t;\boldsymbol{\alpha}_2)]^* dt \\ + \int |s'(t;\boldsymbol{\alpha}_2)|^2 dt - \int |s'(t;\boldsymbol{\alpha}_1)|^2 dt \end{array}}{\sqrt{\int |s''(t;\boldsymbol{\alpha}_1) - s''(t;\boldsymbol{\alpha}_2)|^2 dt}} \tag{41}$$

where $s'(t;\boldsymbol{\alpha})$ is given by (38) and $s''(t;\boldsymbol{\alpha})$ is given by

$$s''(t;\boldsymbol{\alpha}) = \sum_{k=0}^{K-1} \sum_{i=\max(N_1, n-D_k+1)}^{\min(n,N_2-1)} a_{k,i} g_{k,i}(t - iT) \tag{42}$$

which differs from (38) only in the limits of the inner sum. The first symbol index where $\boldsymbol{\alpha}_1 - \boldsymbol{\alpha}_2$ is non-zero corresponds to N_1, and $N_2 = N_1 + R + L - D_{\min}$.

The probability of error can again be bounded using a union bound, similar to (11), where the PED in (41) is substituted as the distance measure in the pairwise error probability. As was the case with the optimal detector, the union bound can then be truncated with a finite number of terms. A good approximation is obtained using (24) with d' used in place of $\tilde{d}$. The distances are listed in Fig. 6(a) for the $K = 1$ case in their unsquared form. Note that many of these distances have negative values. Practically speaking, this means that there are many cases in the detector where an erroneous sequence is closer (in terms of the PED) to the transmitted sequence than the transmitted sequence itself. This is the root cause of the error floor observed in Fig. 7. In Fig. 6(b) the squared distances are listed for the $K = 3$ case along with the optimal squared distances for comparison.

The bit error probability curves generated by the PAM distance measure (41) along with the simulation performance of the three approximations is illustrated in Fig. 7. When $K = 1$ the approximation error is extremely large and there are paths with a negative PED which produce the observed error floor. When $K = 3$ the losses become more acceptable, and when $K = 12$ the losses are negligible. When $K = 48$, (38) is no longer an approximation of (37) and the PAM detector becomes an alternate configuration of MLSD. The performance/complexity trade-off for these PAM detectors is summarized in Table IV. The matched filters are quantified in terms of real-valued length-T filters. For example, the length-$4T$ pulse requires 8 such matched filters to filter the complex-valued received signal in (5).

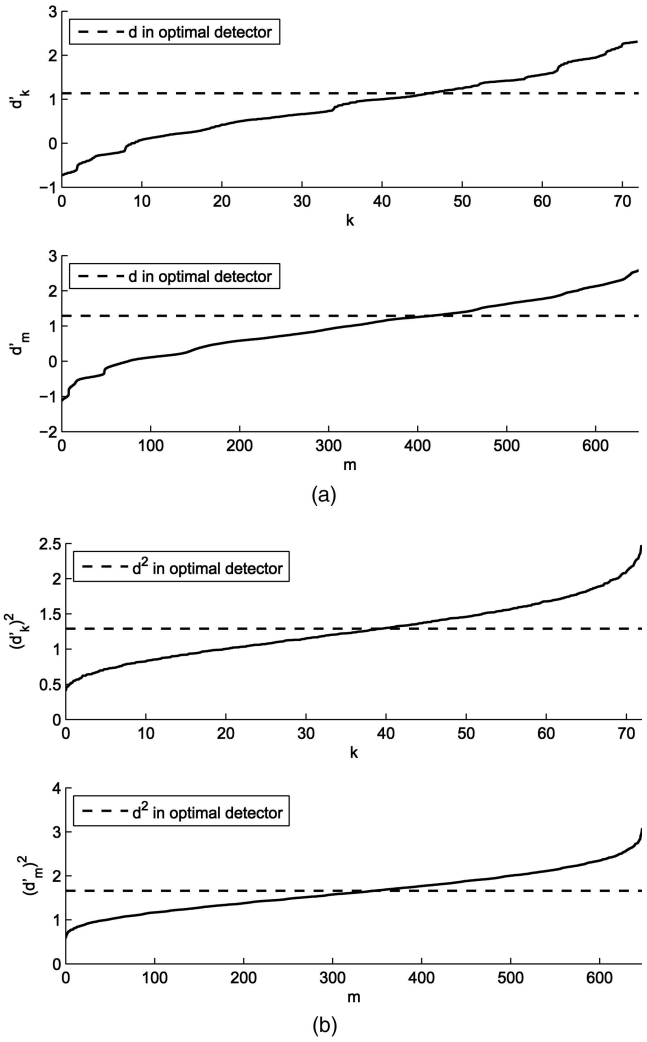

Fig. 6. (a) Values of unsquared distance for PAM approximation with $K = 1$. Note that some of these values are negative, which results in an error floor. (b) Values of squared distance for PAM approximation with $K = 3$.

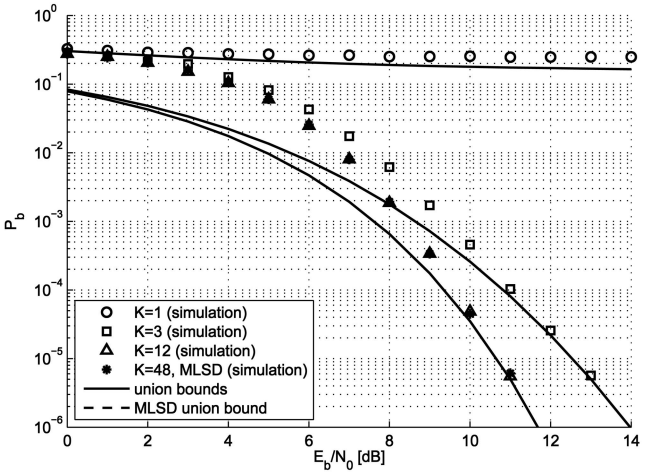

Fig. 7. Performance of PAM-type detectors with $K = 1$, $K = 3$, $K = 12$, and $K = 48$ (MLSD).

TABLE IV
Performance/Complexity Trade-Off for PAM Approximations

Approximation	Number of States	Number of MFs[a]	Loss (dB) at $P_b = 10^{-5}$
$K = 48$	256	128	—
$K = 12$	64	56	0.10
$K = 3$	16	20	1.95
$K = 1$	16	8	∞
$p_{k,i}(t)$	16	20	1.61
$\bar{g}_k(t)$	64	18	0.19

[a]This is the number of equivalent real-valued, length-T filters. This equivalent number is used to facilitate comparisons with the other techniques.

There are other approximations for PAM-based detectors besides truncating the sum in (38). These involve averaging the original set of pulses $\{g_{k,n}(t)\}$ to produce an alternate set of pulses. We highlight two of these averaging schemes.

The first is very similar to the $K = 3$ approximation discussed above. The minimum mean-squared error approximation in [10] is applied to obtain the three pulses $p_{0,i}(t)$, $p_{1,i}(t)$, and $p_{2,i}(t)$, having durations of $4T$, $3T$, and $3T$, respectively. The approximate signal in this case is

$$s'(t;\boldsymbol{\alpha}) = \sum_{k=0}^{2} \sum_{i} a_{k,i} p_{k,i}(t - iT). \tag{43}$$

As with the $K = 3$ approximation, the pseudosymbols associated with these pulses require a trellis of only 16 states, with states defined by

$$\sigma = \{\theta_{n-1}\}. \tag{44}$$

Observe that this trellis is the same as that of frequency pulse truncation with $L' = 1$.

The second averaging scheme is derived directly from the $K = 12$ approximation discussed above. Then the number of pulses is reduced from twelve down to three by averaging the two length-$3T$ pulses to form a single pulse. Similarly, the nine length-$2T$ pulses are averaged to form a single pulse. We also average the multi-h pulses to form the equivalent of single-h pulses. The final pulses are $\bar{g}_0(t)$, $\bar{g}_1(t)$, and $\bar{g}_2(t)$, having durations of $4T$, $3T$, and $2T$, respectively. Note that the subscript i has been dropped from these pulses to reflect their single-h equivalence. The approximate signal in this case is

$$s'(t;\boldsymbol{\alpha}) = \sum_{k=0}^{2} \sum_{i} \bar{a}_{k,i} \bar{g}_k(t - iT) \tag{45}$$

where $\bar{a}_{k,i}$ are a weighted sum of the original pseudosymbols $a_{k,i}$. The remainder of the details for this approximation are in [24]. This 3-pulse approximation, as well as the $K = 12$ approximation upon which it is based, require the 64-state trellis defined by (21).

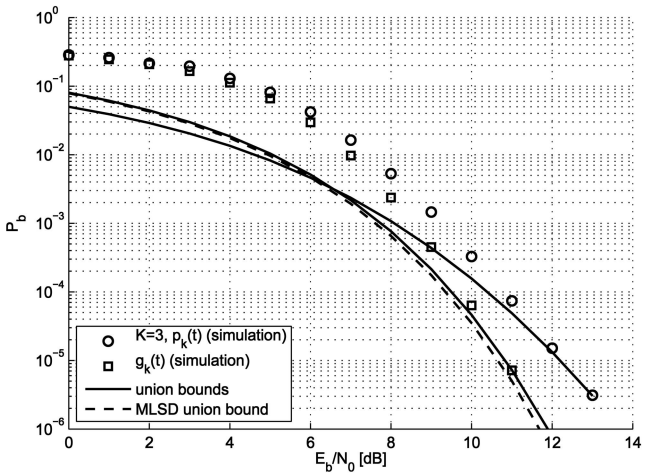

Fig. 8. Performance of PAM-type detectors with averaged pulses.

The performance of these two averaged schemes is shown in Fig. 8. Observe that the minimum mean-squared error approximation performs slightly better than the $K = 3$ approximation in Fig. 7. The 3-pulse scheme with $\bar{g}_k(t)$ performs almost as well as the $K = 12$ approximation in Fig. 7. The probability of bit error curves in Fig. 8 is generated from the PAM distance measure in (41) by substituting the respective approximation, (43) or (45), in the place of (38) (the distances are not shown here, but can be found in [25, ch. 5]). The performance/complexity trade-off for these averaged PAM detectors is also summarized in Table IV.

E. Orthonormal Basis Functions

There have been a number of different methods proposed to decompose CPM signals into a set of orthonormal basis functions. The most recent of these, proposed by Moqvist and Aulin [12], is highlighted here. (For a listing of other approaches of this type, see the references in [12]). The ARTM CPM signal can be exactly represented by

$$s(t;\boldsymbol{\alpha}) = e^{j\vartheta_{n-3}} \sum_{j=1}^{64} c_j(\boldsymbol{\alpha}_n) \varphi_j(t - nT) \tag{46}$$

where $\{\varphi_j(t)\}$ is a set of 64 complex-valued length-T basis functions that span the signal space and $\{c_j(\boldsymbol{\alpha}_n)\}$ is a set of 64×64 complex-valued projection coefficients which map these basis functions into the 64 signals possible signals given by the correlative state vector (4). The goal of this alternate representation is to achieve a reasonably good approximation with only a limited number of basis functions. The approximate signal is given by

$$\tilde{s}(t;\boldsymbol{\alpha}) = e^{j\vartheta_{n-3}} \sum_{j=1}^{H} c_j(\boldsymbol{\alpha}_n) \varphi_j(t - nT) \tag{47}$$

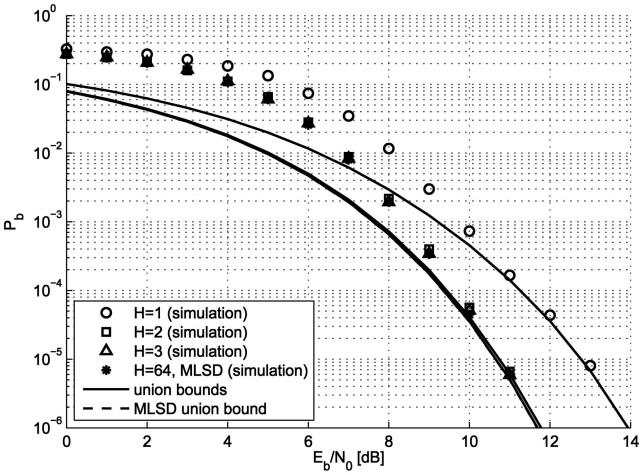

Fig. 9. Performance of detectors with orthogonal basis functions as MFs, where $H = 1$, $H = 2$, $H = 3$, and $H = 64$ (MLSD) basis functions are used.

TABLE V
Performance/Complexity Trade-Off for Orthogonal Basis Function Approximation

H	Number of States	Number of MFs	Loss (dB) at $P_b = 10^{-5}$
64	256	128	—
3	256	12	0.01
2	256	8	0.15
1	256	4	2.20

where $H \leq 64$. This approximation does not reduce the number of trellis states, it only reduces the size of the filter bank. The metric update equation becomes

$$\lambda(n) = \lambda(n-1) + \mathrm{Re}\left[e^{-j\vartheta_{n-3}} \sum_{j=1}^{H} c_j^*(\boldsymbol{\alpha}_n) \int_{nT}^{(n+1)T} r(t)\varphi_j^*(t-nT)dt\right]. \tag{48}$$

The mismatched detector analysis is also used here to characterize the performance of these detectors. Due to the elegance of the signal space decomposition, the squared PED between the signals corresponding to $\boldsymbol{\alpha}_1$ and $\boldsymbol{\alpha}_2$ is given by

$$\hat{d}^2 = \sum_i \sum_{j=1}^{H} |c_j(\boldsymbol{\alpha}_{i,1}) - c_j(\boldsymbol{\alpha}_{i,2})|^2 \tag{49}$$

where the outer sum is non-zero for only $R + L - 1$ values of i. These distance terms are used in a truncated union bound in the same manner as (24) to yield a bit error probability.

The performance of this approximation is shown in Fig. 9. The simulation results coincide with the analytical results for large E_b/N_0 (the numerical values of (49) can be found in [25, ch. 5]). The performance/complexity trade-off is summarized in Table V.

TABLE VI
Complexity-Reduction Properties of Each Proposed Technique

Approximation Type	Phase State Reduction	Correlative State Reduction	MF Reduction
pulse truncation		√	√
SSP	√	√	
PAM		√	√
basis functions			√

IV. COMBINED TECHNIQUES FOR COMPLEXITY REDUCTION

Table VI summarizes the properties of the complexity-reducing techniques described above in terms of whether or not they reduce the number of phase states, correlative states, and/or MFs. From the table it is clear that no single method accomplishes all three types of complexity reduction. However, the table does suggest ways in which these methods may be combined to achieve this end. For example, a frequency pulse truncation-SSP combination leads to phase state reduction, correlative state reduction and MF reduction. Three types of composite approaches are explored in this section. The combinations discussed below were found in an ad hoc manner and not through the use of a systematic approach as in [9] (or Section IIIC). However, these combinations all perform within a few tenths of a dB of optimum and it is not expected that better performing options are available for ARTM CPM. Furthermore, three different 32-state detectors are given that are within one-tenth of a dB of optimum, which is more that one dB better than the 32-state detector that optimizes the SSP design criterion in (29). Based on the quality of the results below, a promising area of future study is the development of a general and systematic approach for combining SSP with the other complexity reduction techniques surveyed herein.

A. Frequency Pulse Truncation and State-Space Partitioning

It has already been established that frequency pulse truncation performs very well for $L' = 2$ and much less so for $L' = 1$. It has also been shown that SSP can reduce the state complexity by a potentially large amount. It is interesting to consider combinations of these two approaches where the complexity savings that result from frequency pulse truncation are leveraged so that SSP does not need to be applied as aggressively as before (recall that in Section IIIC the aggressive use of SSP did not perform as well as the minimum distance results suggested).

We start by using frequency pulse truncation with $L' = 2$ to yield a correlative state reduction, and

combine this with SSP to yield a phase state reduction with the 8-value partition

$$\Gamma^{(8)}(\theta) \triangleq [0\ 1\ 2\ 3\ 4\ 5\ 6\ 7\ 0\ 1\ 2\ 3\ 4\ 5\ 6\ 7]. \quad (50)$$

This results in a 32-state trellis defined by the label vector

$$\epsilon = \{\Gamma^{(8)}(\theta_{n-2}), \Gamma^{(4)}(\alpha_{n-1})\} \quad (51)$$

where the 4-value partition $\Gamma^{(4)}(\alpha_{n-1})$ is used on the data symbols above for notational consistency, not for complexity reduction. (Recall that α_{n-2} is absorbed into the phase state due to the $L' = 2$ approximation.) The performance analysis of this composite detector is based on the mismatched detector analysis using the PED in (23). The two mergers in (14) and (15) are sufficient to characterize the bit error performance using the truncated union bound (24). Note that the analysis in Section IIIC (without pulse truncation) shows that this trellis has $d^2_{\min}(\mathbf{\Gamma}) = 1.272$, and is thus (barely) not considered in the solution of (29).

Another configuration is $L' = 2$ with the 4-value phase state partition

$$\Gamma^{(4)}(\theta) \triangleq [0\ 1\ 2\ 3\ 0\ 1\ 2\ 3\ 0\ 1\ 2\ 3\ 0\ 1\ 2\ 3] \quad (52)$$

which results in the 16-state trellis defined by the label vector

$$\epsilon = \{\Gamma^{(4)}(\theta_{n-2}), \Gamma^{(4)}(\alpha_{n-1})\}. \quad (53)$$

In this case, the analysis in Section IIIC (without pulse truncation) shows that this trellis has $d^2_{\min}(\mathbf{\Gamma}) = 0.651$, which indicates a very poor distance due to $\mathbf{\Gamma}(\Delta\sigma) = 0$ for at least one critical difference state. However, due to the delay in the pulse truncation branch metrics [compare the limits of integration in (9) and (22)], this difference state now becomes only near critical. The bit error analysis must be expanded from the previous case to include the effect of this additional merger, $\boldsymbol{\alpha}_1 - \boldsymbol{\alpha}_2 = \ldots, 0, 2, 0, \ldots$. This merger produces 6 distinct squared distances, ranging from 1.31 to 1.51, and results in a third summation term that is not needed in (24), namely:

$$P_b \approx \frac{7}{(2)(2)(4^5)} \sum_{k=0}^{71} Q\left(\tilde{d}_k \sqrt{\frac{E_b}{N_0}}\right) + \frac{4}{(2)(2)(4^5)} \sum_{m=0}^{647} Q\left(\tilde{d}_m \sqrt{\frac{E_b}{N_0}}\right) + \frac{1}{(2)(2)(4)} \sum_{l=0}^{5} Q\left(\tilde{d}_l \sqrt{\frac{E_b}{N_0}}\right). \quad (54)$$

The performance of these two approximations is shown in Fig. 10. Observe that the 32-state combination has essentially no loss while the 16-state version has a noticeable performance degradation. Note that in Fig. 10, the simulated performance

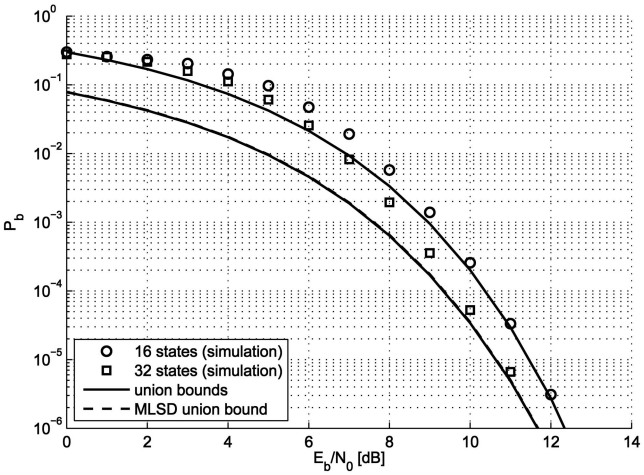

Fig. 10. Performance of detectors using combination of frequency pulse truncation and SSP.

of each detector shows close agreement with the respective union bound (the numerical values of the PED used to generate these bounds are plotted in [25, ch. 5]). This leads to the conclusion that error propagation from the decision feedback, which is used to implement the SSP, has a negligible impact on the performance. Observe also that the 16-state composite detector has a loss of only 0.80 dB, compared with the much larger loss of 4.10 dB in Table II for a 16-state detector using frequency pulse truncation alone.

B. Pulse Amplitude Modulation and State-Space Partitioning

From the earlier discussion of the PAM detectors, a desirable complexity/performance trade-off was achieved using the 3-pulse approximation with $\bar{g}_0(t)$, $\bar{g}_2(t)$, and $\bar{g}_2(t)$. This PAM approximation is now used along with SSP. The first configuration uses $\Gamma^{(8)}(\theta_{n-2})$ and has the 32-state trellis in (51). The performance analysis for this combination is based on the mismatched detector analysis using the PED in (41). The bit error probability is given by

$$P_b \approx \frac{7}{(2)(2)(4^5)} \sum_{k=0}^{71} Q\left(d'_k \sqrt{\frac{E_b}{N_0}}\right) + \frac{4}{(2)(2)(4^5)} \sum_{m=0}^{647} Q\left(d'_m \sqrt{\frac{E_b}{N_0}}\right). \quad (55)$$

The squared PED values in the first summation range from 1.02 to 1.52 and the those in the second summation range from 1.33 to 1.96.

The second combination uses $\Gamma^{(4)}(\theta_{n-2})$, and has the 16-state trellis in (53). The bit error probability for this combination adds an additional term to (55) to account for the additional near-minimum-distance

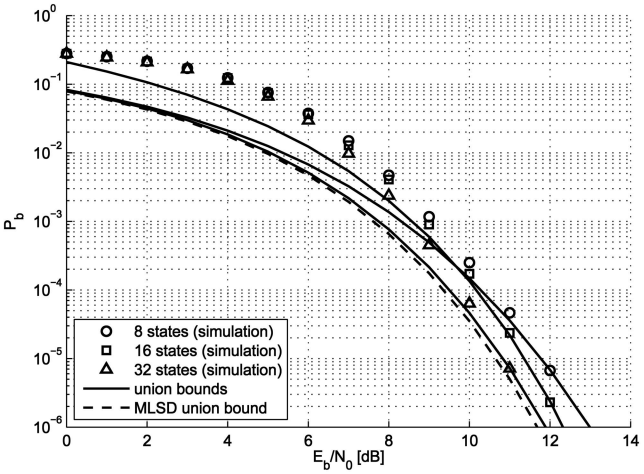

Fig. 11. Performance of detectors using combination of PAM approximations and SSP.

merger:

$$P_b \approx \frac{7}{(2)(2)(4^5)} \sum_{k=0}^{71} Q\left(d'_k \sqrt{\frac{E_b}{N_0}}\right) + \frac{4}{(2)(2)(4^5)} \sum_{m=0}^{647} Q\left(d'_m \sqrt{\frac{E_b}{N_0}}\right) + \frac{1}{(2)(2)(4)} \sum_{l=0}^{5} Q\left(d'_l \sqrt{\frac{E_b}{N_0}}\right). \quad (56)$$

The PED profiles for the first two summations are the same as those in (55). The squared PED values in the third summation range from 1.17 to 5.27.

These first two cases are very similar to the previous example with frequency pulse truncation. The last configuration uses an additional amount of SSP and has an 8-state trellis defined by the label vector

$$\epsilon = \{\Gamma^{(8)}(\theta_{n-2}), \Gamma^{(1)}(\alpha_{n-1})\} \quad (57)$$

where $\Gamma^{(1)}(\alpha)$ is the all-zeros partition. Note that the analysis in Section IIIC (without PAM) shows that this trellis has $d^2_{\min}(\mathbf{\Gamma}) = 0.057$, which is 13.5 dB inferior to the optimal minimum squared distance of 1.288! However, for the PAM-based detector, which has a very large delay in the matched filter computations [see (40)], this difference state is not even near critical. In fact, no additional mergers need to be considered in the bit error approximation, which is given by (55). The only difference from the previous examples is that the numerical values of the PED must be recomputed using the value $N_2 = N_1 + R + L - 1 - D_{\min}$ in (42) to reflect the fact that competing paths merge together one symbol time sooner due to the use of $\Gamma^{(1)}(\alpha_{n-1})$. The PED values in the first summation range from 0.67 to 1.99 and the PED values in the second summation range from 0.91 to 2.53.

The performance of these three detectors is shown in Fig. 11. It is interesting to note that the composite PAM detectors perform better than the composite frequency pulse truncation detectors as the state complexity goes down. The PAM approximation has the additional advantage of having fewer matched filters. The reason the PAM approximation performs well, even when the correlative state vector is severely shortened, is because its MFs (pulses) are longer than one symbol time [11], as shown in (40). In fact, the 8-state trellis in (57) leads to severe losses when attempted using frequency pulse truncation. The performance of the 8-state PAM-SSP detector is approximately 3 dB better than the 8-state SSP detector that optimizes the design criterion in (30). It is not clear from previously published work that results such as these were ever anticipated. Finally, we note that the union bounds in Fig. 11 show close agreement with the simulation results, which indicates that error propagation from the decision feedback does not play a significant role in the performance of these detectors. The numerical values of the PED, used to evaluate (55) and (56), are not shown here but are plotted in [25, ch. 5].

C. Orthogonal Basis Functions and State-Space Partitioning

The last composite configuration considered is the use of orthogonal basis functions with SSP. It has already been shown that SSP can be particularly vulnerable to creating multiple near-minimum-distance error events (mergers), and is also susceptible to error propagation from the decision feedback. It has also been shown that the PAM and frequency pulse truncation approximations are somewhat robust against these effects since their branch metrics are computed with a delay. Neither the standard branch metric (9) or the orthogonal basis function metric (48) have such protection. Therefore, SSP cannot be applied as aggressively with the orthonormal basis functions technique as it was with the PAM or frequency pulse truncation techniques. In fact, the only configuration worth considering here is $H = 3$, with a 32-state trellis defined by the label vector

$$\epsilon = \{\Gamma^{(8)}(\theta_{n-3}), \Gamma^{(1)}(\alpha_{n-2}), \Gamma^{(4)}(\alpha_{n-1})\}. \quad (58)$$

(Note that this trellis has nothing to do with the value of H and can be used with the optimal detector [$H = 64$].) The bit error probability of this technique is given by

$$P_b \approx \frac{7}{(2)(2)(4^5)} \sum_{k=0}^{71} Q\left(\hat{d}_k \sqrt{\frac{E_b}{N_0}}\right) + \frac{4}{(2)(2)(4^5)} \sum_{m=0}^{647} Q\left(\hat{d}_m \sqrt{\frac{E_b}{N_0}}\right) \quad (59)$$

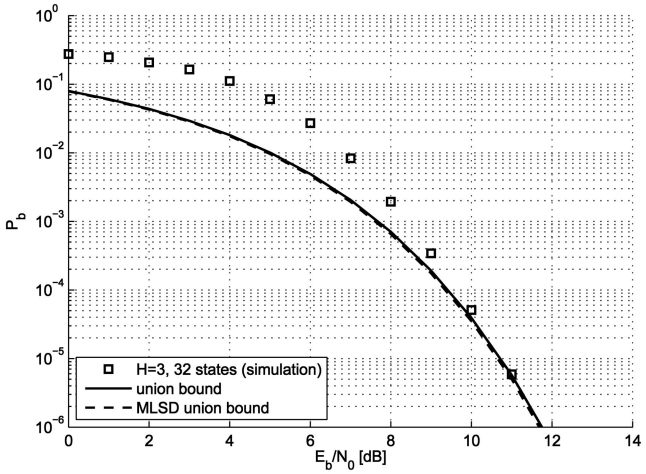

Fig. 12. Performance of 32-state detector using combination of orthogonal basis functions and SSP.

where the PED values $\hat{d}_k$ and $\hat{d}_m$ are given by (49). The squared PED values in the first term range from 1.268 to 1.271 while those in the second term range from 1.631 to 1.636 (the entire set of numerical values is plotted in [25, ch. 5]).

As has already been established, an additional reduction with $\Gamma^{(4)}(\theta_{n-3})$ results in a critical difference state merger with a very poor minimum squared distance of 0.651 (a 2.96 dB loss) and is thus not worth considering. The performance of the 32-state detector is shown in Fig. 12. Observe that this detector has a loss of only 0.02 dB at $P_b = 10^{-5}$ and is the best 32-state detector analyzed in this paper. The fact that this configuration [with $\Gamma^{(8)}(\theta_{n-3})$ and $\Gamma^{(1)}(\alpha_{n-2})$] is better than the 32-state detector that optimizes the SSP design criterion in (29) [with $\Gamma^{(2)}(\theta_{n-3})$ and $\Gamma^{(4)}(\alpha_{n-2})$] underscores the point that designing the trellis to optimize minimum distance alone does not always guarantee the best results.

V. SUMMARY AND CONCLUSIONS

The complexity/performance comparison between the combined methods described in Section IV is summarized in Table VII. Note that the composite PAM detectors perform better than the composite frequency pulse truncation detectors as the state complexity goes down. The PAM approximation has the additional advantage of having fewer matched filters. The 32-state detector based on the combination of orthogonal basis functions and SSP is the best 32-state detector in all categories.

In conclusion, it has been shown that there are two 32-state detectors whose loss in detection efficiency is less than 0.05 dB; two 16-state detectors whose loss in detection efficiency is less than 1 dB; and one 8-state detector whose loss in detection efficiency just greater than 1 dB. These complexity reductions were achieved by a proper combination of complexity reducing techniques. For a given state size, a combination of complexity-reducing techniques always outperforms the use of a single complexity-reducing technique for the cases considered. It is not clear from previously published work that this result was ever anticipated. The analysis and simulation results presented in this paper can be used to guide real implementations that strive to achieve a target complexity/performance goal for ARTM CPM.

TABLE VII
Performance/Complexity Trade-Off for Various Combinations of Reduced-Complexity Detectors

Approximation	Number of States	Number of MFs	Loss (dB) at $P_b = 10^{-5}$
MLSD	256	128	—
$L' = 2$, $\Gamma^{(8)}(\theta)$	32	32	0.05
$L' = 2$, $\Gamma^{(4)}(\theta)$	16	32	0.80
PAM, $\Gamma^{(8)}(\theta)$	32	18	0.08
PAM, $\Gamma^{(4)}(\theta)$	16	18	0.60
PAM, $\Gamma^{(8)}(\theta)$, $\Gamma^{(1)}(\alpha)$	8	18	1.05
$H = 3$, $\Gamma^{(8)}(\theta)$	32	12	0.02

REFERENCES

[1] Chalfant, T., and Irving, C.
Range telemetry improvement and modernization.
In *Proceedings of the International Telemetering Conference*, Las Vegas, NV, Oct. 1997, 294–303.

[2] Gao, W., and Feher, K.
FQPSK: A bandwidth and RF power efficient technology for telemetry applications.
In *Proceedings of the International Telemetering Conference*, Las Vegas, NV, Oct. 1997, 480–488.

[3] Hill, T.
An enhanced, constant envelope, interoperable shaped offset QPSK (SOQPSK) waveform for improved spectral efficiency.
In *Proceedings of the International Telemetering Conference*, San Diego, CA, Oct. 2000, 127–136.

[4] Range Commanders Council Telemetry Group, Range Commanders Council, White Sands Missile Range, NM
IRIG Standard 106-00: Telemetry Standards, 2000.
(Available on-line at http://www.ntia.doc.gov/osmhome/106.pdf).

[5] Law, E., and Feher, K.
FQPSK versus PCM/FM for aeronautical telemetry applications; Spectral occupancy and bit error probability comparisons.
In *Proceedings of the International Telemetering Conference*, Las Vegas, NV, Oct. 1997, 489–496.

[6] Hill, T.
Performance of SOQPSK and multi-h CPM in the presence of adjacent cahannel interference.
In *Proceedings of the International Telemetering Conference*, Las Vegas, NV, Oct. 2001, 255–263.

[7] Aulin, T., Sundberg, C-E., and Svensson, A.
Viterbi detectors with reduced complexity for partial response continuous phase modulation..
In *Proceedings of the National Telecommunications Conference* (NTC'81), New Orleans, LA, Nov./Dec. 1981, A7.6.1–A7.6.7.

[8] Svensson, A., Sundberg, C-E., and Aulin, T.
A class of reduced-complexity Viterbi detectors for partial response continuous phase modulation.
IEEE Transactions on Communications, **32** (Oct. 1984), 1079–1087.

[9] Larsson, T.
Optimal design of CPM decoders based on state-space partitioning.
In *Proceedings of the International Conference on Communications, ICC'93*, Geneva, Switzerland, May 1993, 123–127.

[10] Perrins, E., and Rice, M.
PAM decomposition of M-ary multi-h CPM.
IEEE Transactions on Communications, **53**, 12 (Dec. 2005), 2065–2075.

[11] Perrins, E., and Rice, M.
A new performance bound for PAM-based CPM detectors.
IEEE Transactions on Communications, **53**, 10 (Oct. 2005), 1688–1696.

[12] Moqvist, P., and Aulin, T.
Orthogonalization by principal components applied to CPM.
IEEE Transactions on Communications, **51** (Nov. 2003), 1838–1845.

[13] Anderson, J. B., Aulin, T., and Sundberg, C-E.
Digital Phase Modulation.
New York: Plenum Press, 1986.

[14] Rimoldi, B. E.
A decomposition approach to CPM.
IEEE Transactions on Information Theory, **34** (Mar. 1988), 260–270.

[15] Geoghegan, M.
Description and performance results for a multi-h CPM telemetry waveform.
In *Proceedings of IEEE MILCOM*, **1** (Oct. 2000), 353–357.

[16] Aulin, T.
Breadth-first maximum likelihood sequence detection: Basics.
IEEE Transactions on Communications, **47**, 2 (Feb. 1999), 208–216.

[17] Aulin, T.
Breadth-first maximum likelihood sequence detection: Geometry.
IEEE Transactions on Communications, **51**, 6 (June 2003), 2071–2080.

[18] Eyuboglu, M. V., and Qureshi, S. U.
Reduced-state sequence estimation with set partitioning and decision feedback.
IEEE Transactions on Communications, **36**, 1 (Jan. 1988), 13–20.

[19] Larsson, T.
A state-space partitioning approach to trellis decoding.
Ph.D. dissertation, Chalmers University of Technology, Göteborg, Sweden, Dec. 1991.

[20] Laurent, P. A.
Exact and approximate construction of digital phase modulations by superposition of amplitude modulated pulses (AMP).
IEEE Transactions on Communication, **34** (Feb. 1986), 150–160.

[21] Mengali, U., and Morelli, M.
Decomposition of M-ary CPM signals into PAM waveforms.
IEEE Transactions on Information Theory, **41** (Sept. 1995), 1265–1275.

[22] Kaleh, G. K.
Simple coherent receivers for partial response continuous phase modulation.
IEEE Journal on Selected Areas of Communications, **7** (Dec. 1989), 1427–1436.

[23] Colavolpe, G., and Raheli, R.
Reduced-complexity detection and phase synchronization of CPM signals.
IEEE Transactions on Communication, **45** (Sept. 1997), 1070–1079.

[24] Perrins, E., and Rice, M.
Optimal and reduced complexity receivers for M-ary multi-h CPM.
In *Proceedings of the IEEE Wireless Communications and Networking Conference* (WCNC'04), Atlanta, GA, Mar. 2004, 1165–1170.

[25] Perrins, E.
Reduced complexity detection methods for continuous phase modulation.
Ph.D. dissertation, Brigham Young University, Provo, UT, Aug. 2005.

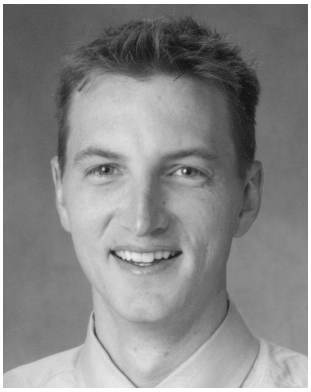

Erik Perrins (S'96—M'05—SM'06) received his B.S. (1997, magna cum laude), his M.S. (1998), and his Ph.D. (2005) all from Brigham Young University, Provo, UT.

From 1998–2004 he was with Motorola, Inc. in Schaumburg, IL where he worked on advanced development of land mobile radio products. Since 2004 he has been an industry consultant on receiver design problems such as synchronization and complexity reduction. He joined the faculty in the Department of Electrical Engineering & Computer Science at the University of Kansas in August 2005. His research interests are in digital communication theory, synchronization, channel coding, and complexity reduction in receivers.

Dr. Perrins is a member of the IEEE Communications Society.

Michael Rice (M'82—SM'98) received a B.S.E.E. from Louisiana Tech University, Ruston, in 1987 and his Ph.D. from Georgia Tech, Atlanta, in 1991. He was with Digital Transmission Systems, Inc. in Atlanta and joined the faculty at Brigham Young University in 1991 where he is currently the Jim Abrams Professor in the Department of Electrical & Computer Engineering. He was a NASA/ASEE Summer Faculty Fellow at the Jet Propulsion Laboratory during 1994 and 1995 where he worked on land mobile satellite systems. During the 1999–2000 academic year, Professor Rice was a visiting scholar at the Communication Systems and Signal Processing Institute at San Diego State University. His research interests are in the area of digital communication theory and error control coding with a special interest in applications to telemetering and software radio design. He has been a consultant to both government and industry on telemetry related issues.

Dr. Rice was chair of the Utah section of IEEE from 1997 to 1999 and chair of the Signal Processing & Communications Society Chapter of the Utah section from 2002 to 2003. He is currently serving as the vice-chair of the Communication Theory Technical Committee in the IEEE Communications Society and as Technical Editor for Command, Control and Communication Systems for *IEEE Transactions on Aerospace and Electronic Systems*. He is a member of the IEEE Communications Society.